Semiconducting Enriched Carbon Nanotube Aligned Arrays of Tunable Density and Their Electrical Transport Properties

Biddut K. Sarker,[†,‡] Shashank Shekhar,[†,‡] and Saiful I. Khondaker[†,‡,§,*]

[†]Nanoscience Technology Center, [‡]Department of Physics, and [§]School of Electrical Engineering and Computer Science, University of Central Florida, 12424 Research Parkway, Suite 400, Orlando, Florida 32826, United States

ABSTRACT We demonstrate assembly of solution-processed semiconducting enriched (99%) single-walled carbon nanotubes (s-SWNTs) in an array with varying linear density *via* ac dielectrophoresis (DEP) and investigate detailed electronic transport properties of the fabricated devices. We show that (i) the quality of the alignment varies with frequency of the applied voltage and that (ii) by varying the frequency and concentration of the solution, we can control the linear density of the s-SWNTs in the array from 1/μm to 25/μm. The DEP assembled s-SWNT devices provide the opportunity to investigate the transport property of the arrays in the direct transport regime. Room temperature electron transport measurements of the fabricated devices show that with increasing nanotube density the device mobility increases while the current on−off ratio decreases dramatically. For the dense array, the device current density was 16 μA/μm, on-conductance was 390 μS, and sheet resistance was 30 kΩ/$\square$. These values are the best reported so far for any semiconducting nanotube array.

KEYWORDS: semiconducting carbon nanotube · aligned array · solution-processed · dielectrophoresis · transistors

Due to their exceptional electronic properties including very high mobility, near ballistic conductance, and resistance against electromigration, single-walled carbon nanotubes (SWNTs) are considered to be a promising building block for future digital and analog electronics.[1,2] Devices fabricated from arrays of SWNTs can be advantageous as they average out device-to-device inhomogeneity of individual SWNTs and cover large areas. In addition, devices fabricated with nanotube arrays contain hundreds of parallel SWNTs contributing to charge transport, which can increase current outputs up to hundreds of microamperes. The degree of alignment and the density of SWNT in the array are expected to have a great influence on device performance.[3−13] For these reasons, there is a significant research effort to fabricate devices with massively parallel arrays of SWNTs for field effect transistors (FETs),[3−7,14] RF applications,[9,10,15] plastic electronics,[16,17] display technologies,[18] electrodes,[19,20] and sensors.[21]

The aligned arrays of SWNTs have been achieved using either direct growth *via* chemical vapor deposition (CVD)[5,9,10,22−26] or post-growth from solution-processed assembly techniques.[3,4,18−20,27,28] However, such arrays contain a mixture of both semiconducting nanotubes (s-SWNT, 67%) and metallic nanotubes (m-SWNT, 33%), and the electric transport property of the arrays is dominated by the metallic pathways. In order to obtain better transistor properties, it is essential to selectively remove metallic nanotubes from the arrays *via* electrical breakdown.[3−5,26,29] Using this method, improved FET performance has been demonstrated; however, the device mobility was calculated without examining the number of nanotubes remaining in the device after electrical breakdown. In addition, in this method, it is assumed that individual metallic nanotubes can be removed selectively without affecting the neighboring nanotubes. Recent investigations reveal that removal of such a large number of nanotubes *via* electrical breakdown may have a detrimental effect on the remaining nanotubes in the array. For example, Wang *et al.* have shown that although the on−off ratio of FET was improved by electrical breakdown, the on-current was decreased more (around 90%) than what was expected (33%) from breaking of metallic nanotubes.[26] Recently, we have shown that in a high-density nanotube array, the electrical breakdown of one nanotube affects adjacent nanotubes due to the formation of dipole fields at the tip of the broken nanotube. This leads to a highly correlated breakdown of neighboring

* Address correspondence to saiful@ucf.edu.

Received for review April 9, 2011 and accepted July 13, 2011.

Published online July 13, 2011
10.1021/nn201314t

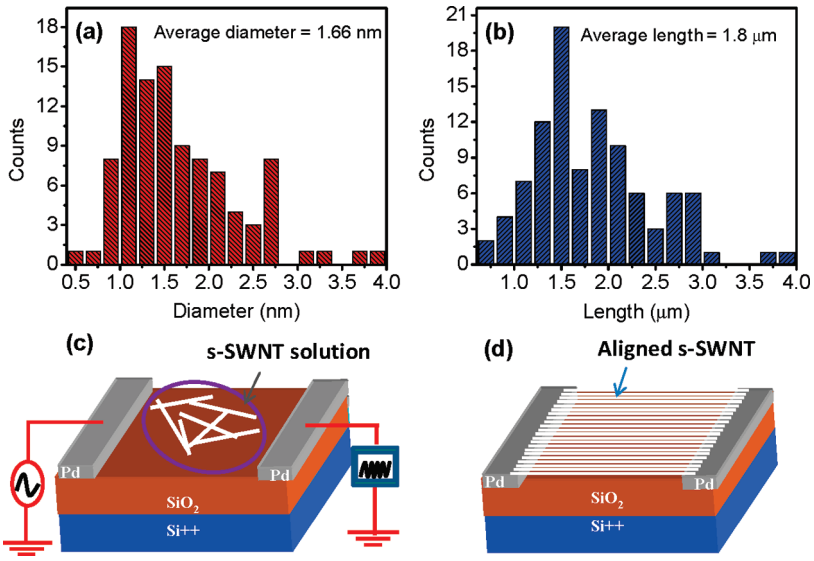

Figure 1. (a) Diameter distribution of the s-SWNT in the solution. The average diameter is 1.6 nm. (b) Length distribution of the s-SWNT. The average length is 1.8 μm. (c) Schematic of dielectrophoretic assembly of s-SWNT. A 3 μL of liquid droplet of s-SWNT solution was dispersed, and an ac voltage of 5 V with varying frequency is applied between source and drain electrodes. (d) Schematic of nanotube alignment between palladium source and drain electrodes.

nanotubes, and semiconducting nanotubes are not immune to correlated breakdown.[30] Therefore, the removal of a large number of metallic nanotubes through electrical breakdown is a challenging and imperfect approach.[15,30,31] In this respect, it is important to fabricate devices consisting mostly of semiconducting nanotubes by minimizing or eliminating the metallic transport pathways where semiconducting enriched nanotubes hold the key.

Recently, it has been shown that a solution-based sorting technique such as density gradient ultracentrifugation can provide highly enriched (99%) s-SWNTs in aqueous solution. A few studies have been reported on the FET fabrication using a random network of such enriched s-SWNTs where transport occurs through the percolative pathways.[32−34] Compared to random networks where tube−tube junction limits charge transport, a perfectly aligned 2D array is expected to exhibit electronic properties that approached intrinsic properties of the individual nanotubes. Engel *et al.* have used evaporation-driven self-assembly to obtain a 2D aligned s-SWNT array with a nanotube density of ~10−20 s-SWNT/μm, which have shown a sheet resistance of ~200 kΩ/□ and on-conductance of ~25 μS.[35] It is generally believed that the device property can be further improved if the density of the nanotube in the arrays can be increased further. In addition, it is also of great importance to investigate the electrical properties in the direct transport regime with varying density of s-SWNT for many practical applications.

In this paper, we demonstrate controlled assembly of semiconducting single-walled carbon nanotube arrays of tunable density from a high-quality semiconducting enriched (99%) aqueous solution using ac dielectrophoresis (DEP). We show that the quality of the alignment of the s-SWNT varies with frequency of the applied voltage. By varying the frequency and s-SWNT solution concentration, we can control the linear density of the nanotubes in the array from 1 s-SWNT/μm to 25 s-SWNT/μm. The room temperature electron transport measurements of the fabricated FETs using the aligned array show that, with increasing nanotube density, the device mobility increases while the current on−off ratio dramatically decreases. For the device with a dense array, the current density is 16 μA/μm, on-conductance is 390 μS, and sheet resistance is 30 kΩ/□. These values are the best reported so far for any semiconducting nanotube array. We also discuss possible reasons for low current on−off ratio at high linear density.

RESULTS AND DISCUSSION

The nanotube assembly was done using dielectrophoresis (DEP) from a high-purity (99%) s-SWNT aqueous solution purchased from NanoIntegris.[36] The diameter of the nanotubes varied from 0.5 to 3.9 nm with an average of 1.6 nm, and the length of the nanotubes varied from 0.7 to 4.0 μm with an average value of 1.8 μm as measured by atomic force microscopy (AFM) (Figure 1a,b) (also see Supporting Information Figure S1). Figure 1c shows a schematic of the DEP assembly setup. The assembly was performed in a probe station between prefabricated palladium (Pd) source and drain electrodes of channel length $L = 2$ μm and channel width $W = 25$ μm. The original solution has a s-SWNT concentration of 10 μg/mL and was further diluted to a desired concentration using deionized (DI) water (see details in Materials and Methods section). For the assembly, a small (3 μL) drop of the s-SWNT solution was cast onto the chip containing electrode pairs.

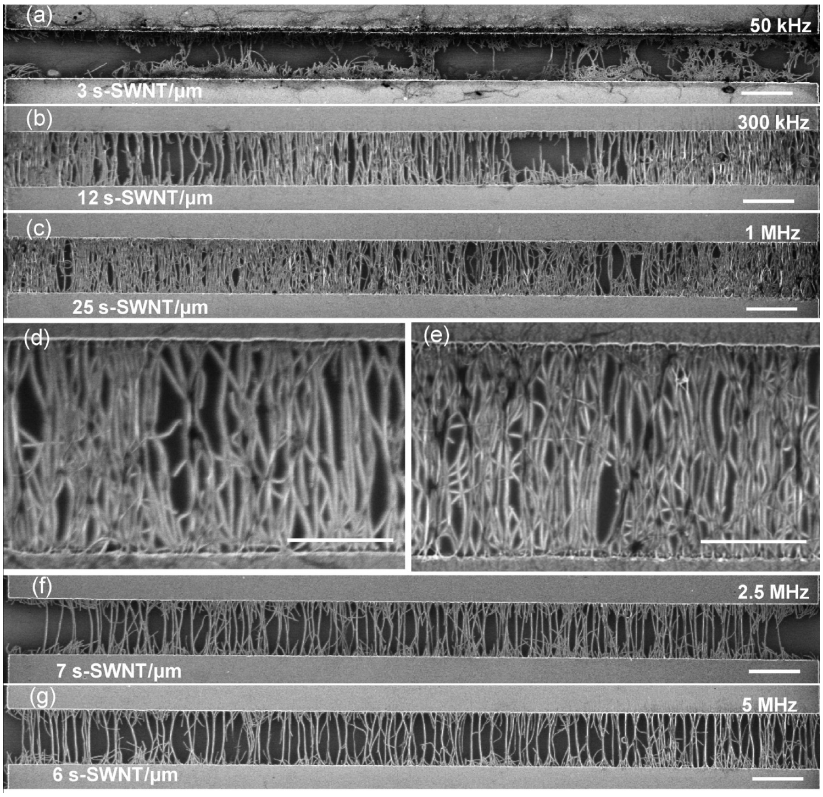

Figure 2. SEM image showing frequency dependence of s-SWNT assembly for a fixed solution concentration of 100 ng/mL at (a) 50 kHz, (b) 300 kHz, (c) 1 MHz, (f) 2.5 MHz, and (g) 5 MHz. Scale bars: 2 μm. (d,e) Magnified image of (b) and (c). Scale bars: 1 μm. The corresponding linear densities of the s-SWNTs in the array are (a) 3 s-SWNT/μm, (b) 12 s-SWNT/μm, (c) 25 s-SWNT/μm, (f) 7 s-SWNT/μm, and (g) 6 s-SWNT/μm.

A fixed ac voltage ($V_{p\text{-}p}$) of 5 V was applied between source and drain electrodes for 40 s. The frequency was varied from 50 kHz to 5 MHz to study the quality of the assembled s-SWNT array. The ac field gives rise to a time-averaged DEP force, making the nanotubes move in a translational motion along the electric field gradient and align the nanotubes in the direction of the electric field lines (Figure 1d). We demonstrated in the past that DEP assembly technique is an effective approach to fabricate devices using 2D, 1D, and 0D nanomaterials.[3,4,37−41] DEP can be advantageous over other solution-processed techniques because it allows the materials to be directly integrated to prefabricated electrodes at the selected positions of the circuits and does not require postetching or transfer printing.

After the DEP assembly, scanning electron microscopy (SEM) was used to characterize the arrays. Figure 2 shows SEM images of s-SWNT assemblies at different frequencies for a fixed solution concentration of 100 ng/mL. It can be clearly seen from these images that the number of assembled nanotubes between the electrodes and the quality of the assembly strongly depends on the frequency of the applied voltage. At 50 kHz, a large number of short nanotubes are anchored to the electrode bases without bridging the electrode gap (Figure 2a). Although there are a few nanotubes that completely bridged the electrodes, however, the alignment quality is poor. In addition, some aggregation can also be seen. The quality of the assembly and their orientation is improved significantly when the frequency is increased to 300 kHz. This is shown in Figure 2b. In this assembly, a large number of individual nanotubes bridged the electrodes. This can be more clearly seen from the magnified images in Figure 2d. A majority of the nanotubes are reasonably aligned along with a few misaligned nanotubes. Although the nanotubes' lengths vary from 0.7 to 4 μm in the solution, it is seen from the images that most of the bridged nanotubes' lengths are equal to the electrode gap. This suggests that the DEP process favors the alignment of nanotubes of length comparable to the electrode gap. One major drawback of the assembly at 300 kHz is that the distribution of the nanotube along the channel width is not uniform and some voids are seen. The more uniform distribution of nanotubes along with increased number of nanotubes in the assembly was achieved when the frequency was increased to 1 MHz (Figure 2c). A magnified view of this assembly is presented in Figure 2e. Although a majority of the nanotubes are aligned within $\pm 15^\circ$ of the longitudinal axis, some nanotubes were misaligned and went over the aligned nanotubes. Further increase in frequency to 2.5 and 5 MHz (Figure 2f,g) resulted in a

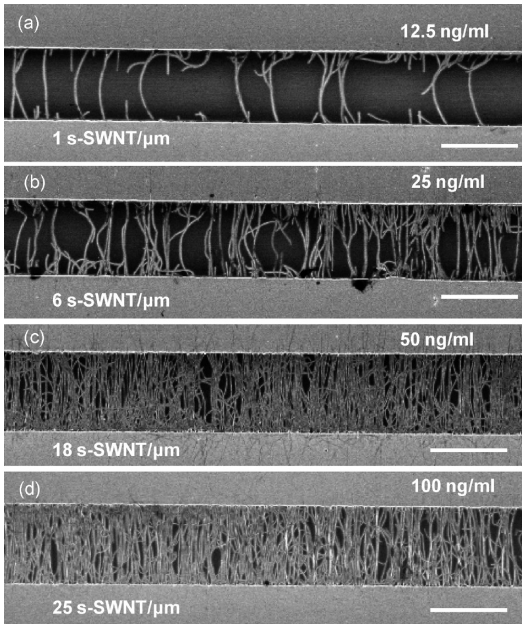

Figure 3. Solution concentration dependence of s-SWNT assembly at a fixed frequency of 1 MHz. SEM images show assembled nanotubes for solution concentrations of (a) 12.5 ng/mL, (b) 25 ng/mL, (c) 50 ng/mL, (d) 100 ng/mL. Scale bar: 2 μm. The corresponding s-SWNT densities are 1 s-SWNT/μm, 6 s-SWNT/μm, 18 s-SWNT/μm, and 25 s-SWNT/μm.

better alignment; however, the number of nanotubes bridging the electrodes decreased. In addition, some short nanotubes can be seen at the electrodes' bases due to the electric field line alternation near nanotube–electrode junctions.[3]

From these SEM images, we counted the total number of individual nanotubes that completely bridged the source and drain electrodes and divided the total by channel width to calculate the average linear density (D) of s-SWNT arrays. For the solution concentration of 100 ng/mL, the value of D at 50 kHz, 300 kHz, 1 MHz, 2.5 MHz, and 5 MHz are 3 s-SWNT/μm, 12 s-SWNT/μm, 25 s-SWNT/μm, 7 s-SWNT/μm, and 6 s-SWNT/μm, respectively. From these images, it is clear that with increasing frequency the quality of the alignment improves; however, the density of nanotubes initially increases with frequency and then decreases. We have done similar frequency-dependent studies at other solution concentrations of 12.5, 25, 50, and 100 ng/mL.

We have also investigated how the concentration of the s-SWNT solution affects the assembly. Figure 3 shows SEM images for the DEP assembled s-SWNT array for solution concentrations of 12.5, 25, 50, and and 100 ng/mL at a fixed frequency of 1 MHz. When the solution concentration is 12.5 ng/mL (Figure 3a), the average density is 1 s-SWNT/μm. Figure 3b,c shows SEM images of the array with solution concentrations of 25 and 50 ng/mL, respectively. It is seen from these images that the number of assembled nanotubes is increased with solution concentration. The average densities are 6 s-SWNT/μm and ~18 s-SWNT/μm for a concentration of 25 and 50 ng/mL, respectively. As the solution concentration is increased to 100 ng/mL (Figure 3c), we found that the linear density of nanotubes increased to ~25 s-SWNT/ μm. We have studied similar concentration-dependent DEP assemblies at other frequencies of 50 kHz, 300 kHz, 2.5 MHz, and 5 MHz, and the corresponding nanotube densities were recorded from their respective SEM images (not shown here).

Figure 4 summarizes the DEP assembly of s-SWNT at different solution concentrations and different frequencies. Figure 4a shows how the density varies with solution concentrations. For a fixed frequency, the number of nanotubes increases with solution concentrations. Figure 4b shows the histogram of nanotube density with frequency at different solution concentrations. The maximum density of nanotubes is found at 1 MHz for all solution concentrations, and it decreases both at lower and at higher frequencies. From here, it can be seen that, by tuning the frequency and solution concentration, we can vary the linear density of the s-SWNTs in the array from 1 s-SWNT/μm to 25 s-SWNT/μm.

The variation of the linear density of s-SWNT with frequency can be explained by DEP theory. Considering the nanotubes are cylindrical shape, the DEP force (F_{DEP}) exerted on a nanotube is given by[42] $F_{DEP} \propto \varepsilon_m \mathrm{Re}[(\varepsilon_n^* - \varepsilon_m^*)/\varepsilon_m^*]\nabla E^2$, where $\varepsilon_{n,m}^* = \varepsilon_{n,m} - i\sigma_{n,m}/\omega$ with ε_n and ε_m as the dielectric constants of s-SWNT and medium, respectively, σ_n and σ_m are the conductivity of s-SWNT and medium, respectively, and E is the electric field. Figure 4c shows a plot of F_{DEP} *versus* frequency where we have used $\sigma_n = 0.35$ S/m,[43] $\sigma_m = 4 \times 10^{-4}$ S/m,[44] $\varepsilon_n = 2.5$,[45] and $\varepsilon_m = 78$.[46] We note that, although our s-SWNT solution is ionic surfactant based, we have used the conductivity of DI water as a medium conductivity as the original s-SWNT solution was diluted by at least 100 times with DI water for the assembly. From this plot, we see that the F_{DEP} decreases with frequency >0.2 MHz, whereas our experiment shows that the linear density decreases above 1 MHz. The small variation could be due to a small uncertainty of the values of different parameters used in the calculation. Although the F_{DEP} *versus* frequency plot shows fairly good agreement with our experimental observation at high frequency range, it does not explain our observation in low frequency range as it shows that F_{DEP} is constant at low frequency. This is because, at low frequency range, the F_{DEP} is screened by electric double layers of ions on the electrode surface, and this needs to be taken into account to get the effective DEP force.[47−50] When nanotube solution is placed onto the electrode surface and ac voltage is applied, the electrodes get polarized and electric double layers are formed at electrode/solution interface due to two parallel layers of charge separation.

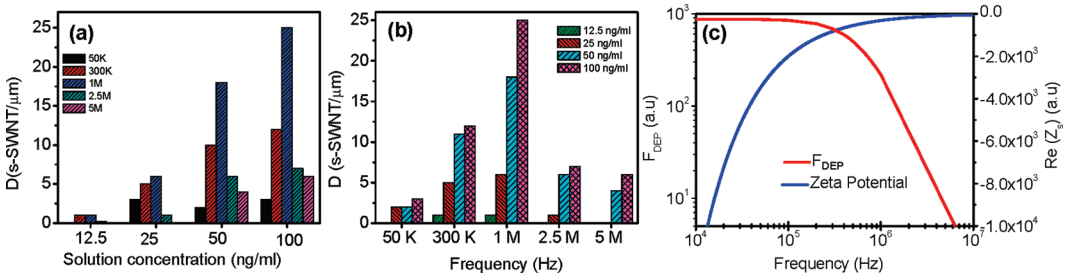

Figure 4. (a) Variation of linear density of s-SWNTs in the array with solution concentrations at frequency of 50 kHz, 300 kHz, 1 MHz, 2.5 MHz, and 5 MHz. (b) Histogram shows variation linear density of s-SWNT with frequency at solution concentrations of 12.5, 25, 50, and 100 ng/mL. Maximum linear density is about 25 s-SWNT/μm in the frequency range of 300 kHz to 1 MHz. Linear density of s-SWNT is decreased both at high and at low frequencies. (c) Plot of DEP force (left axis) *versus* frequency for s-SWNT (red solid line). Plot of zeta-potential (right axis) *versus* frequency (blue solid line) that opposes the DEP force.

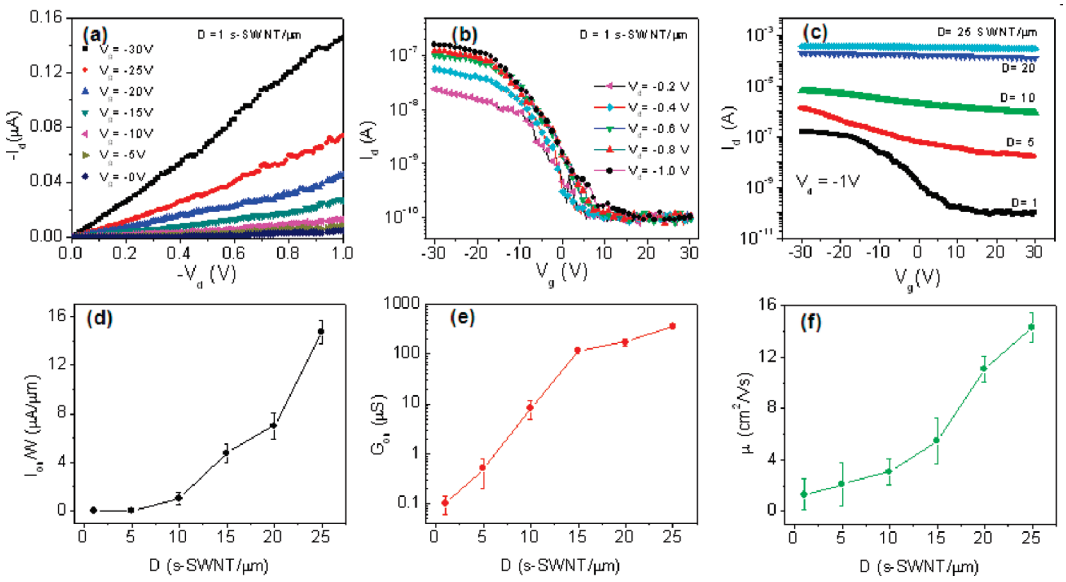

Figure 5. (a) Output characteristics (I_d-V_d) of the best FET device with linear density of 1 s-SWNT/μm at $V_g = 0$ to -30 V with a -5 V interval. (b) Transfer characteristics (I_d-V_g) of the same device at $V_d = -0.2$ to -1 V with a -0.2 V interval. (c) I_d-V_g curves at $V_d = -1$ V of the aligned array FET devices with nanotube densities of 1, 5, 10, 20, and 25 s-SWNT/μm. (d) Variation of the normalized on-current with nanotube densities. (e) Plot of on-conductance of the devices *versus* nanotube density in the array. (f) Plot of mobility *versus* density of nanotubes in the device.

The first layer is the surface charges of the electrodes, and the second layer is composed of the ions attracted to surface charge. As a result, a potential (known as zeta-potential) is formed between the electrode/solution interface. The zeta-potential is proportional to electric double layer impedance (Z) and is modeled as $Z = 1/C_d(i\omega)^P$, where C_d is capacitance between the solution and electrodes and p is the power factor.[47] Figure 4c (blue curve) shows a plot of the zeta-potential as a function of frequency where we have taken the reported C_d and p value for DI water as 50 nF and 0.8, respectively.[47] This plot clearly shows that at low frequency the electric double layer strongly opposes the DEP force and at about 1 MHz the zeta-potential diminishes. This is in agreement with our experimental observation.

To evaluate the electrical performance of the fabricated s-SWNT arrays with different nanotube densities, we have measured room temperature electronic transport properties in back-gated FET configuration. Figure 5a is a plot of drain current (I_d) as a function of source–drain voltage (V_d) of the best device with 1 s-SWNT/μm at gate voltages $V_g = 0$ to -30 V with a -5 V interval. The curve shows linear behavior of I_d with V_d, consistent with other short channel SWNT FET devices.[35] In addition, the linear behavior of the I_d-V_d curves at small V_d bias indicates that the Ohmic contact is formed between s-SWNTs and Pd electrodes. Figure 5b shows transfer characteristics (I_d *versus* V_g plot) of the same device at $V_d = -0.2$ to -1 V, with a -0.2 interval. The device shows p-type field effect behavior with a well modulation with V_g. All of the measured devices with different nanotube densities have shown similar output and transfer characteristics; however, the gate modulations as well as magnitude of their current values were different. Figure 5c exhibits the transfer characteristics of our best devices with nanotube densities of 1, 5, 10, 20, and 25 s-SWNT/μm.

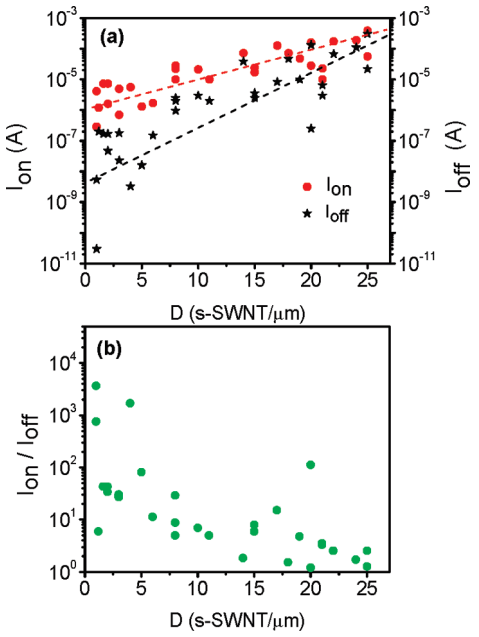

Figure 6. (a) On-current (red circle) and off-current (black star) variation as a function of number of SWNTs/μm in the array. (b) Plot of current on/off ratio *versus* number of SWNTs/μm.

All of the devices were measured at a fixed $V_d = -1$ V. We see from this figure that the I_d of the device with 1 s-SWNT/μm is changed by several orders of magnitude with V_g with a current on−off ratio of 1.5×10^3. However, as the nanotube density is increased in the devices, the current on−off ratio decreased. This will be discussed in more detail in Figure 6.

Another important observation in Figure 5c is that the on-current I_{on} (at $V_g = -30$ V) increases with nanotube density. This can be more clearly seen in Figure 5d, where we plot normalized on-current (I_{on}/W) *versus* nanotube density, where I_{on} was measured at $V_d = -1$ V and $V_g = -30$ V. The maximum I_{on}/W = 15.6 μA/μm reported here is the highest reported for any semiconducting nanotube network and is a manifestation of remarkable properties of our dense s-SWNT array (25 s-SWNT/μm). The on-state conductance ($G_{on} = I_{on}/V_d$) *versus* nanotube density plot (Figure 5e) shows the G_{on} also increases with nanotube density. In addition, it can be seen from this figure that the device with 25 s-SWNTs/μm has a maximum G_{on} of 390 μS with a corresponding sheet resistance (R_s) of 30 kΩ/$\square$. The maximum G_{on} of our device is 16 times higher and the minimum R_s values are 6 times lower than that of previous reported values of semiconducting nanotube array devices with comparable device geometry ($L = 4$ μm).[35] The highest G_{on}, highest I_{on}/W, and lowest R_s for our most dense array device are expected because our devices were fabricated with a higher nanotube density in the array (25 s-SWNT/μm) and with shorter channel length. In addition, the electronic transport occurs directly through individual s-SWNTs without any percolation through nanotube junctions.

Figure 5f shows the measured linear mobility (μ) of all of the devices as a function of nanotube density. The linear mobility is calculated using the standard formula $\mu = (L/WC_iV_d)(dI_d/dV_g)$, where dI_d/dV_g is the transconductance extracted from the slope of the transfer curve (see also Supporting Information Figure S2), $C_i = D/[C_Q^{-1} + (1/2\pi\varepsilon_0\varepsilon)\ln[\sinh(2\pi t_{ox}D)/\pi Dr]]$ is the specific capacitance per unit area of aligned array,[4,5] where C_Q is the quantum capacitance of the nanotube (=4×10^{-10} F/m), t_{ox} is the oxide thickness (=250 nm), ε is the dielectric constant of SiO_2 (3.9), ε_0 is the permittivity in the free space (8.85×10^{-12} F/m), and r is the averages radius of the nanotubes. It can be seen from Figure 5e that the mobility increases with nanotube density, similar to what has been reported for random network of s-SWNTs.[34] The maximum mobility of our devices (16 cm^2/V·s) is slightly lower than the previous reported maximum mobility (20 cm^2/V·s) of s-SWNT aligned array devices of comparable channel length.[35] This is small variation could be attributed to several factors: (a) our device channel length (2 μm) is smaller than the device channel length (4 μm) of ref 35, and it has been reported that higher channel length gives higher mobility.[33] (b) In our device, we have used a bottom gate with a high t_{ox} (250 nm), while in ref 35, the devices were fabricated in top gate configuration with thin t_{ox} (15 nm).

In order to further investigate the effect of nanotube density on the device performance, the current on/off ratio I_{on}/I_{off}, the on-current I_{on}, and off-current I_{off} of all the measured devices are plotted as a function of nanotube density in Figure 6. The plot of I_{on} and I_{off} with nanotube density (Figure 6a) shows that I_{on} (red circle) increases with the nanotube density. On the other hand, I_{off} (black star) is also increased with nanotube density. In addition, a large variation of I_{off} is seen for the device with lower nanotube density. The plot of on/off ratio *versus* nanotube density (Figure 6b) demonstrates that devices with low density (~1 s-SWNTs/μm) exhibit a on/off ratio as high as ~10^4, although a large device-to-device variation from 7 to 10^4 can be seen. However, the on−off ratio and their variations decrease significantly with increasing nanotube density. This may be due to several reasons. One possible reason could be the presence of a small number of m-SWNTs in the array. The solution that was used for s-SWNT assembly contains 1% m-SWNT, and it has been speculated in the past that m-SWNTs may be more favorable during the DEP assembly process.[43,45] In order to estimate the possible fraction of m-SWNT in our DEP assembled array, we have carried out DEP assembly of individual s-SWNTs in a taper-shaped electrode design and measured their electrical transport properties. A representative SEM image of this assembly is shown in Figure 7a. Figure 7b is a

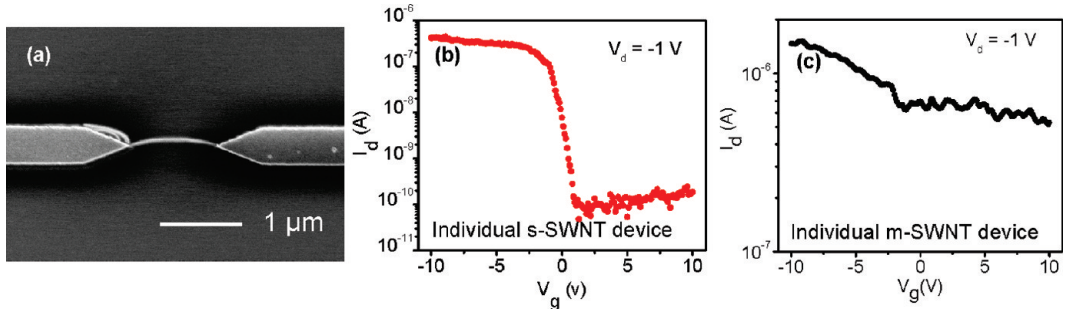

Figure 7. SEM image of an individual s-SWNT device. The I_d-V_g curve of a typical individual (b) s-SWNT device and (c) m-SWNT device. The current on−off ratios of s-SWNT and m-SWNT devices are 5×10^3 and 3, respectively. The bias voltage in the both curves was $V_d = -1$ V.

TABLE 1. Estimate of the Current On−Off Ratio of the Aligned Array FETs as a Function of Possible Number of m-SWNTs in the Array[a]y

1 s-SWNT/μm = 25 s-SWNT		4 s-SWNT/μm = 100 s-SWNT		8 s-SWNT/μm = 200 s-SWNT		25 s-SWNT/μm = 625 s-SWNT	
*m-SWNT	on/off	*m-SWNT	on/off	*m-SWNT	on/off	*m-SWNT	on/off
0	10000	1	102	2	102	6	106
1	26	2	52	4	52	12	54
2	15	3	35	6	35	18	30

[a] The on-currents for s-SWNT and m-SWNT are 4×10^{-7} and 1.5×10^{-6} A, respectively. The off-currents for s-SWNT and m-SWNT are 8×10^{-11} and 5×10^{-7} A, respectively. Note: *m-SWNT denotes the most probable number of m-SWNTs in the arrays.

I_d-V_g curve of a typical individual s-SWNT device with on-current ($I_{s,on}$) $\sim 4 \times 10^{-7}$ A, off-current ($I_{s,off}$) $\sim 8 \times 10^{-11}$ A, and current on−off ratio of 5×10^3. The I_d-V_g curve of a typical m-SWNT presented in Figure 7c shows the on−off ratio of 3 with on-current ($I_{m,on}$) $\sim 1.5 \times 10^{-6}$ A and off-current ($I_{m,off}$) $\sim 5 \times 10^{-7}$A. The details study of this individual s-SWNT assembly will be discussed elsewhere. The electrical measurement data of 87 such individual devices show that 85 nanotubes are semiconducting (on/off ratio $\geq$10) and 2 nanotubes are metallic (on/off ratio <10). Using this individual assembly as a guide, we estimate that there may be up to 3% nanotubes in the array which could be metallic. In order to understand how this small percentage of m-SWNT can affect the property of the array, we estimated the on−off ratio of our aligned array using $I_{on}/I_{off} = (sI_{s,on} + mI_{m,on})/(sI_{s,off} + mI_{m,off})$, where s and m are the number of s-SWNTs and m-SWNTs, respectively, in the array. Table 1 summarizes the estimated on−off ratio of the FETs as function of probable number of m-SWNTs in the arrays. It can be seen from the table that for the array with 1 s-SWNT/μm (total 25 s-SWNTs), if there is no m-SWNT present, the I_{on}/I_{off} ratio is limited by the off-current of s-SWNT, and I_{on}/I_{off} could be 10 000. However, if we consider that there may be two m-SWNTs, the I_{on}/I_{off} ratio is decreased to 15. For the array with 1 s-SWNT/μm (total 25 s-SWNTs), it is possible that some devices may contain no m-SWNT and some devices may contain 1 or 2 m-SWNTs, so a large variation in I_{on}/I_{off} is not unreasonable. On the other hand, for the array of 25 s-SWNT/μm (total 625 s-SWNTs), it is almost certain that there may be a few m-SWNTs. So the on−off ratio can vary from 106 to 30 for different percentage of m-SWNTs. However, our experimental data at higher density array show that the on−off ratio is less than 10, which is not completely consistent with this model.

The possible reason for lower on−off ratio of the devices with higher nanotube densities could be due to the electrostatic screening effect of the gate voltage.[35,51,52] For the devices with higher nanotube density, the gate thickness (250 nm) is larger than internanotube spacing and the electric field lines of the nanotubes are screened by neighboring nanotubes.[51,53,54] Therefore, the gate voltage cannot deplete completely the charge carriers in the nanotubes, which results in the high off-current and turns to a lower on−off ratio of the devices.

In summary, we have demonstrated for the first time that semiconducting nanotubes can be controllably aligned with a linear density from 1 s-SWNTs/μm to 25 s-SWNTs/μm by dielectrophoresis. The alignment densities were controlled independently by varying solution concentration and frequency of the applied electric field. At both low and high frequency limits, s-SWNT alignment density is low and it is higher in the frequency range of 300 kHz to 1 MHz. We found that the performance of the fabricated FETs is strongly influenced by s-SWNT density in the device. The devices fabricated with highest density nanotube have shown the lowest sheet resistance, the highest on-conductance, and the highest on-current density.

We also observed that device mobility is increased with nanotube density, and the highest device mobility 16 $cm^2/V \cdot s$ reported here is rather high considering the channel length (2 μm) of our devices. The current on/off ratio of the FET devices decreases with increasing nanotube density, which can be attributed to the possible presence of a tiny fraction of m-SWNTs and the electrostatics screening effect. Our study has important implications for the large-scale fabrication of FET devices with semiconducting carbon nanotubes.

MATERIALS AND METHODS

The 99% s-SWNT aqueous solution was purchased from NanoIntegris, and it was free from catalytic particles and stable for at least 6 months.[36] The original solution has a s-SWNT concentration of ~10 μg/mL, and it was diluted 100, 200, 400, and 800 times using deionized (DI) water to prepared concentrations of 100, 50, 25, and 12.5 ng/mL, respectively.

The directed assembly of s-SWNTs at predefined palladium electrodes was done in a probe station under ambient conditions *via* DEP. Pd electrodes were fabricated on heavily doped silicon substrates capped with a thermally grown 250 nm thick SiO_2 layer using standard EBL followed by deposition of Cr (3 nm) and Pd (27 nm) and standard lift off. Prior to the assembly, the electrodes were placed in an oxygen plasma cleaner for 10 min to remove any unwanted organic residues on the surface. Pd was used because it is known to make the best electrical contact to SWNTs. The channel lengths (L) were 2 μm, and the channel width (W) was 25 μm. For the assembly, a small (3 μL) droplet of the s-SWNT solution was cast onto the chip containing the nine electrode pairs by a micropipet. A function generator (BK Precision 4011A) was used to supply an ac voltage of $V_{p\text{-}p} = 5$ V, with varying frequencies of 50 kHz, 300 kHz, 1 MHz, 2.5 MHz, and 5 MHz between the source and drain electrodes for $t = 40$ s. The signals were monitor by a dual trace oscilloscope (BK Precision 2120B). After 40 s, the function generator was turned off and the remaining solution was blown out from the chip using a nitrogen gas flow.

The electrical transport measurements of the s-SWNT arrays were carried out by DL Instruments 1211 current preamplifier and a Keithley 2400 source meter interfaced with LabView program. The SEM images of s-SWNT assembly were taken on Zeiss Ultra-55 SEM using Inlens detector with an accelerating voltage ~1 kV. Trapping mode AFM images were acquired using Dimension 3100 AFM (Veeco).

Acknowledgment. The help from E. Jimenez, E. Silbar, and N. Kang is greatly appreciated. This work is partially supported by the U.S. National Science Foundation under Grant ECCS-0748091 (CAREER).

Supporting Information Available: (1) AFM image and height profile of semiconducting nanotubes. (2) Variations of normalized transcendence with nanotube density. This material is available free of charge *via* the Internet at http://pubs.acs.org.

REFERENCES AND NOTES

1. Saito, R.; Dresselhaus, G.; Dresselhaus, M. S. *Physical Properties of Carbon Nanotubes*; World Scientific: Singapore, 1998.
2. Avouris, P.; Chen, Z.; Perebeinos, V. Carbon-Based Electronics. *Nat. Nanotechnol.* **2007**, *2*, 605–615.
3. Shekhar, S.; Stokes, P.; Khondaker, S. I. Ultrahigh Density Alignment of Carbon Nanotube Arrays by Dielectrophoresis. *ACS Nano* **2011**, *5*, 1739–1746.
4. Stokes, P.; Silbar, E.; Zayas, Y. M.; Khondaker, S. I. Solution Processed Large Area Field Effect Transistors from Dielectrophoreticly Aligned Arrays of Carbon Nanotubes. *Appl. Phys. Lett.* **2009**, *94*, 113104-1–113104-3.
5. Kang, S. J.; Kocabas, C.; Ozel, T.; Shim, M.; Pimparkar, N.; Alam, M. A.; Rotkin, S. V.; Rogers, J. A. High-Performance Electronics Using Dense, Perfectly Aligned Arrays of Single-Walled Carbon Nanotubes. *Nat. Nanotechnol.* **2007**, *2*, 230–236.
6. Ryu, K.; Badmaev, A.; Wang, C.; Lin, A.; Patil, N.; Gomez, L.; Kumar, A.; Mitra, S.; Wong, H.-S. P.; Zhou, C. CMOS-Analogous Wafer-Scale Nanotube-on-Insulator Approach for Submicrometer Devices and Integrated Circuits Using Aligned Nanotubes. *Nano Lett.* **2009**, *9*, 189–197.
7. Kocabas, C.; Pimparkar, N.; Yesilyurt, O.; Kang, S. J.; Alam, M. A.; Rogers, J. A. Experimental and Theoretical Studies of Transport through Large Scale, Partially Aligned Arrays of Single-Walled Carbon Nanotubes in Thin Film Type Transistors. *Nano Lett.* **2007**, *7*, 1195–1202.
8. Ishikawa, F. N.; Curreli, M.; Olson, C. A.; Liao, H.-I.; Sun, R.; Roberts, R. W.; Cote, R. J.; Thompson, M. E.; Zhou, C. Importance of Controlling Nanotube Density for Highly Sensitive and Reliable Biosensors Functional in Physiological Conditions. *ACS Nano* **2010**, *4*, 6914–6922.
9. Kocabas, C.; Kim, H.-s.; Banks, T.; Rogers, J. A.; Pesetski, A. A.; Baumgardner, J. E.; Krishnaswamy, S. V.; Zhang, H. Radio Frequency Analog Electronics Based on Carbon Nanotube Transistors. *Proc. Natl. Acad. Sci. U.S.A.* **2008**, *105*, 1405–1409.
10. Kocabas, C.; Dunham, S.; Cao, Q.; Cimino, K.; Ho, X.; Kim, H.-S.; Dawson, D.; Payne, J.; Stuenkel, M.; Zhang, H.; *et al.* High-Frequency Performance of Submicrometer Transistors That Use Aligned Arrays of Single-Walled Carbon Nanotubes. *Nano Lett.* **2009**, *9*, 1937–1943.
11. Snow, E. S.; Novak, J. P.; Campbell, P. M.; Park, D. Random Networks of Carbon Nanotubes as an Electronic Material. *Appl. Phys. Lett.* **2003**, *82*, 2145–2147.
12. Kumar, S.; Murthy, J. Y.; Alam, M. A. Percolating Conduction in Finite Nanotube Networks. *Phys. Rev. Lett.* **2005**, *95*, 066802-1–066802-4.
13. Kumar, S.; Pimparkar, N.; Murthy, J. Y.; Alam, M. A. Theory of Transfer Characteristics of Nanotube Network Transistors. *Appl. Phys. Lett.* **2006**, *88*, 123505-1–123505-3.
14. LeMieux, M. C.; Roberts, M.; Barman, S.; Jin, Y. W.; Kim, J. M.; Bao, Z. Self-Sorted, Aligned Nanotube Networks for Thin-Film Transistors. *Science* **2008**, *321*, 101–104.
15. Rutherglen, C.; Jain, D.; Burke, P. Nanotube Electronics for Radio Frequency Applications. *Nat. Nanotechnol.* **2009**, *4*, 811–819.
16. Ishikawa, F. N.; Chang, H.-k.; Ryu, K.; Chen, P.-c.; Badmaev, A.; De Arco, L. G.; Shen, G.; Zhou, C. Transparent Electronics Based on Transfer Printed Aligned Carbon Nanotubes on Rigid and Flexible Substrates. *ACS Nano* **2009**, *3*, 73–79.
17. Feng, C.; Liu, K.; Wu, J.-S.; Liu, L.; Cheng, J.-S.; Zhang, Y.; Sun, Y.; Li, Q.; Fan, S.; Jiang, K. Flexible, Stretchable, Transparent Conducting Films Made from Superaligned Carbon Nanotubes. *Adv. Funct. Mater.* **2010**, *20*, 885–891.
18. Opatkiewicz, J.; LeMieux, M. C.; Bao, Z. Nanotubes on Display: How Carbon Nanotubes Can Be Integrated into Electronic Displays. *ACS Nano* **2010**, *4*, 2975–2978.
19. Sarker, B. K.; Liu, J.; Zhai, L.; Khondaker, S. I. Fabrication of Organic Field Effect Transistor by Directly Grown Poly(3-hexylthiophene) Crystalline Nanowires on Carbon Nanotube Aligned Array Electrode. *ACS Appl. Mater. Interfaces* **2011**, *3*, 1180–1185.
20. Sarker, B. K.; Islam, M. R.; Alzubi, F.; Khondaker, S. I. Fabrication of Aligned Carbon Nanotube Array Electrodes for Organic Electronics Devices. *Mater. Express* **2011**, *1*, 80–85.
21. Kim, S. N.; Rusling, J. F.; Papadimitrakopoulos, F. Carbon Nanotubes for Electronic and Electrochemical Detection of Biomolecules. *Adv. Mater.* **2007**, *19*, 3214–3228.
22. Hong, S. W.; Banks, T.; Rogers, J. A. Improved Density in Aligned Arrays of Single-Walled Carbon Nanotubes by

Sequential Chemical Vapor Deposition on Quartz. *Adv. Mater.* **2010**, *22*, 1826–1830.
23. McNicholas, T. P.; Ding, L.; Yuan, D.; Liu, J. Density Enhancement of Aligned Single-Walled Carbon Nanotube Thin Films on Quartz Substrates by Sulfur-Assisted Synthesis. *Nano Lett.* **2009**, *9*, 3646–3650.
24. Zhou, W.; Ding, L.; Yang, S.; Liu, J. Synthesis of High-Density, Large-Diameter, and Aligned Single-Walled Carbon Nanotubes by Multiple-Cycle Growth Methods. *ACS Nano* **2011**, *5*, 3849–3857.
25. Ding, L.; Yuan, D.; Liu, J. Growth of High-Density Parallel Arrays of Long Single-Walled Carbon Nanotubes on Quartz Substrates. *J. Am. Chem. Soc.* **2008**, *130*, 5428–5429.
26. Wang, C.; Ryu, K.; Arco, L. G. D.; Badmaev, A.; Zhang, J.; Lin, X.; Che, Y.; Zhou, C. Synthesis and Device Applications of High-Density Aligned Carbon Nanotubes Using Low-Pressure Chemical Vapor Deposition and Stacked Multiple Transfer. *Nano Res.* **2010**, *3*, 831–842.
27. Li, X.; Zhang, L.; Wang, X.; Shimoyama, I.; Sun, X.; Seo, W.-S.; Dai, H. Langmuir−Blodgett Assembly of Densely Aligned Single-Walled Carbon Nanotubes from Bulk Materials. *J. Am. Chem. Soc.* **2007**, *129*, 4890–4891.
28. Yu, G.; Cao, A.; Lieber, C. M. Large-Area Blown Bubble Films of Aligned Nanowires and Carbon Nanotubes. *Nat. Nanotechnol.* **2007**, *2*, 372–377.
29. Collins, P. G.; Arnold, M. S.; Avouris, P. Engineering Carbon Nanotubes and Nanotube Circuits Using Electrical Breakdown. *Science* **2001**, *292*, 706–709.
30. Shekhar, S.; Erementchouk, M.; Leuenberger, M. N.; Khondaker, S. I. Correlated Breakdown of Carbon Nanotubes in an Ultra-high Density Aligned Array. *Appl. Phys. Lett.* **2011**, *98*, 243121-1–243121-3.
31. Liao, A.; Alizadegan, R.; Ong, Z.-Y.; Dutta, S.; Xiong, F.; Hsia, K. J.; Pop, E. Thermal Dissipation and Variability in Electrical Breakdown of Carbon Nanotube Devices. *Phys. Rev. B* **2010**, *82*, 205406-1–205406-9.
32. Wang, C.; Zhang, J.; Ryu, K.; Badmaev, A.; De Arco, L. G.; Zhou, C. Wafer-Scale Fabrication of Separated Carbon Nanotube Thin-Film Transistors for Display Applications. *Nano Lett.* **2009**, *9*, 4285–4291.
33. Wang, C.; Zhang, J.; Zhou, C. Macroelectronic Integrated Circuits Using High-Performance Separated Carbon Nanotube Thin-Film Transistors. *ACS Nano* **2010**, *4*, 7123–7132.
34. Rouhi, N.; Jain, D.; Zand, K.; Burke, P. J. Fundamental Limits on the Mobility of Nanotube-Based Semiconducting Inks. *Adv. Mater.* **2011**, *23*, 94–99.
35. Engel, M.; Small, J. P.; Steiner, M.; Freitag, M.; Green, A. A.; Hersam, M. C.; Avouris, P. Thin Film Nanotube Transistors Based on Self-Assembled, Aligned, Semiconducting Carbon Nanotube Arrays. *ACS Nano* **2008**, *2*, 2445–2452.
36. http://www.nanointegris.com/.
37. Stokes, P.; Khondaker, S. I. High Quality Solution Processed Carbon Nanotube Transistors Assembled by Dielectrophoresis. *Appl. Phys. Lett.* **2010**, *96*, 083110-1–083110-3.
38. Stokes, P.; Khondaker, S. I. Local-Gated Single-Walled Carbon Nanotube Field Effect Transistors Assembled by AC Dielectrophoresis. *Nanotechnology* **2008**, *17*, 175202-1–175202-5.
39. Joung, D.; Chunder, A.; Zhai, L.; Khondaker, S. I. High Yield Fabrication of Chemically Reduced Graphene Oxide Field Effect Transistor by Dielectrophoresis. *Nanotechnology* **2010**, *21*, 165202-1–165202-5.
40. Khondaker, S. I. Fabrication of Nanoscale Device Using Individual Colloidal Gold Nanoparticle. *IEE Proc.: Circuits Devices Syst.* **2004**, *151*, 457–460.
41. Khondaker, S. I.; Luo, K.; Yao, Z. Fabrication of Single-Electron Transistors Using Dielectrophoretic Trapping of Individual Gold Nanoparticles. *Nanotechnology* **2010**, *21*, 095204-1–095204-4.
42. Dimaki, M.; Boggild, P. Dielectrophoresis of Carbon Nanotubes Using Microelectrodes: A Numerical Study. *Nanotechnology* **2004**, *15*, 1095–1102.
43. Krupke, R.; Hennrich, F.; Kappes, M. M; Lohneysen, H. V. Surface Conductance of Induced Dielectrophoresis of Semiconducting Single-Walled Carbon Nanotubes. *Nano Lett.* **2004**, *4*, 1395–1399.
44. Pedrosa, A.; Serrano, M. L. Solubilities of Sodium Gluconate in Water and in Aqueous Solutions of Ethanol and Methanol. *J. Chem. Eng. Data* **2000**, *45*, 461–463.
45. Krupke, R.; Hennrich, F.; Weber, H. B.; Kappes, M. M.; Lohneysen, H. V. Simultaneous Deposition of Metallic Bundles of Single-Walled Carbon Nanotubes Using AC-Dielectrophoresis. *Nano Lett.* **2003**, *3*, 1019–1023.
46. Duchamp, M.; Lee, K.; Dwir, B.; Seo, J. W.; Kapon, E.; Forro, L. S.; Magrez, A. Controlled Positioning of Carbon Nanotubes by Dielectrophoresis: Insights into the Solvent and Substrate Role. *ACS Nano* **2010**, *4*, 279–284.
47. Burg, B. R.; Bianco, V.; Schneider, J.; Poulikakos, D. Electrokinetic Framework of Dielectrophoretic Deposition Devices. *J. Appl. Phys.* **2010**, *107*, 124308-1–124308-11.
48. Castellanos, A.; Ramos, A.; Gonzalez, A; Green, N. G.; Morgan, H. Electrohydrodynamics and Dielectrophoresis in Microsystems: Scaling Laws. *J. Phys. D: Appl. Phys.* **2003**, *36*, 2584–2597.
49. Uppalapati, M; Huang, Y. M.; Jackson, T. N.; Hancock, W. O. Microtubule Alignment and Manipulation Using AC Electrokinetics. *Small* **2008**, *4*, 1371–1381.
50. Zhou, H.; Preston, M. A.; Tilton, R. D.; White, L. R. Calculation of the Dynamic Impedance of the Double Layer on a Planar Electrode by the Theory of Electrokinetics. *J. Colloid Interface Sci.* **2005**, *292*, 277–289.
51. Kshirsagar, C.; Hong, L.; Kopley, T. E.; Banerjee, K. Accurate Intrinsic Gate Capacitance Model for Carbon Nanotube-Array Based FETs Considering Screening Effect. *Electron Device Lett.* **2008**, *29*, 1408–1411.
52. Cao, Q.; Xia, M.; Kocabas, C.; Shim, M.; Rogers, J. A.; Rotkin, S. V. Gate Capacitance Coupling of Singled-Walled Carbon Nanotube Thin-Film Transistors. *Appl. Phys. Lett.* **2007**, *90*, 023516-1–023516-3.
53. Snow, E. S.; Campbell, P. M.; Ancona, M. G.; Novak, J. P. High Mobility Carbon Nanotubes Thin Film Transistors on a Polymeric Substrate. *Appl. Phys. Lett.* **2005**, *86*, 033105-1–033105-3.
54. Jing, G.; Sebastien, G.; Mark, L.; Supriyo, D. Metal-Insulator-Semiconductor Electrostatics of Carbon Nanotubes. *Appl. Phys. Lett.* **2002**, *81*, 1486–1488.